Journal of Nuclear Materials xxx (2013) xxx–xxx

Contents lists available at SciVerse ScienceDirect

Journal of Nuclear Materials

journal homepage: www.elsevier.com/locate/jnucmat

Varying the pre-discharge lithium wall coatings to alter the characteristics of the ELM-free H-mode pedestal in NSTX

D.P. Boyle [a,*], J.M. Canik [b], R. Maingi [b,1], P.B. Snyder [c], T.H. Osborne [c], the NSTX Team

[a] Princeton University, Princeton, NJ 08543, USA
[b] Oak Ridge National Laboratory, Oak Ridge, TN 37831, USA
[c] General Atomics, San Diego, CA 92121, USA

ARTICLE INFO

Article history:
Available online xxxx

ABSTRACT

A previous experiment in the National Spherical Torus Experiment (NSTX) showed that pre-discharge lithium deposition gradually suppressed edge-localized modes (ELMs) and had nearly continuous relationships with reduced recycling and transport. In this paper, additional data filled gaps in the earlier experiment, and demonstrates that recycling, confinement, and pedestal structure continued to improve with additional lithium, *even after ELMs were completely suppressed*. New analysis shows that toroidal rotation and ion temperature also increased continuously with additional lithium. Besides its evolution with additional lithium, we also characterize the time evolution of the ELM-free H-mode pedestal as average density rose and impurities accumulated. We find that the pedestal structure, divertor heat flux and D_α profiles, and inferred recycling coefficient did not change significantly, at least until radiative losses become dominant. This suggests that the low-recycling properties of lithium were not significantly degraded over the duration of the discharge.

1. Introduction

Lithium has attracted significant interest as a plasma-facing material, both for its potential as a low-Z liquid metal and for its property of bonding hydrogenic species and reducing plasma recycling [1]. Lithium wall conditioning in the National Spherical Torus Experiment (NSTX) [2] was motivated by improved performance in previous experiments [3,4]. The success of lithium coatings is evident in their steadily increased use [5–7] to the point of being used in the majority of NSTX discharges. Improvements in performance following lithium coatings included increased discharge duration and confinement and achievement of high-confinement (H-mode) discharges in which edge-localized mode (ELM) instabilities were completely suppressed [5–10]. Despite greatly improved confinement and steady divertor power loads, these ELM-free H-mode discharges are not considered a model for future devices because they continuously accumulated carbon impurities that would normally be ejected periodically by ELMs. In addition, nearly all NSTX H-mode discharges demonstrated an increase in average density with time, though it increased more slowly with lithium coatings. However, it may be possible to overcome these limitations with methods such as pulsed 3-D fields [11,12] or the "snowflake" divertor configuration [13].

This paper combines data from several experimental runs: an experiment where pre-discharge lithium coatings gradually increased from 0 to 930 mg over 22 H-mode discharges, and two short, more recent experiments where lithium deposition varied from 430 to 570 mg over 7 total H-mode discharges. Elements of the first experiment have been described previously [8,9,14–19]; it was the first experiment to use the upgraded dual evaporator LITER lithium deposition system [8,10] and began with an entirely lithium-free baseline. In that experiment, medium triangularity ($\delta \sim 0.5$) discharges with lithium coatings >400 mg and neutral beam power $P_{NBI} = 4$ MW reached global stability limits and disrupted at ~0.3 s. Heating power was reduced over the next few discharges until a sustained discharge was attained with $P_{NBI} = 2$ MW. Thus the more recent discharges with $P_{NBI} = 1.2–3$ MW were necessary to fill the gap in the original data between 350 and 715 mg of Li. Unlike the first set of experiments, these discharges were performed with significant quantities of passivated lithium already in the vacuum vessel and did not use helium glow discharge cleaning between shots.

Previous work has reported on many aspects of the original lithium scan: the gradual suppression of ELMs [9], the stabilization of kink/peeling modes that cause ELMs [14], the continuous reduction in transport at the pedestal top [15,16], the systematic modification of the pedestal profiles [17], and the continuous evolution of recycling and confinement with increasing lithium deposition

* Corresponding author. Address: Princeton Plasma Physics Laboratory, PO Box 451, Princeton, NJ 08543-0451, USA.
E-mail addresses: dboyle@pppl.gov (D.P. Boyle), rmaingi@pppl.gov (R. Maingi).
[1] Presenting author.

0022-3115/$ - see front matter © 2013 Elsevier B.V. All rights reserved.
http://dx.doi.org/10.1016/j.jnucmat.2013.01.213

[18,19]. However, the effect of additional lithium beyond the point of ELM suppression on plasma profiles and performance was not determined, due to the gap in the original data. Questions also remained about the pumping persistence of the lithium coatings under the deuterium fluence of an extended discharge.

In Section 2 of this paper, we characterize the evolution of ELM-free discharges with varying pre-discharge lithium deposition. With the addition of the newer data and new analysis of the ion profiles, we demonstrate that the global and pedestal parameters continued to improve with additional lithium, *even after ELMs were completely suppressed*. In Section 3, we analyze the temporal evolution of these discharges as average density rose and impurities accumulated. We find that the pedestal structure, divertor heat flux and D_α emission profiles, and inferred recycling coefficient did not change significantly, at least until radiative losses become dominant. In Section 4, we discuss the implications and questions raised by these results.

2. Evolution with increasing lithium

Previous work [18,19] showed that global indicators of recycling decreased and performance increased nearly continuously with increasing lithium deposition. Fig. 1 shows that these trends continued with additional lithium even after ELMs were completely suppressed. Two indicators of recycling, D_α emission from the lower divertor and neutral pressure at the midplane, decreased nearly continuously with increasing lithium deposition. Because the more recent discharges used different sightlines and calibrations, panels (a) and (b) only use data from the original scan. These measurements were made at ~0.3 s before some of the ELM-free discharges reached global stability limits, so there is no gap in the data The line-averaged density at $t \sim 0.4$ s also decreased nearly continuously in panel (c), which includes the new data with 400–600 mg of Li deposition. Stored energy and normalized beta (not shown) were just as high in the ELM-free discharges with $P_{NBI} = 1.2$–3 MW as the ELMy discharges with $P_{NBI} = 4$ MW. The beam power dependence is accounted for by using the scaled H97L confinement factor [20], which increased continuously with lithium deposition in panel (d).

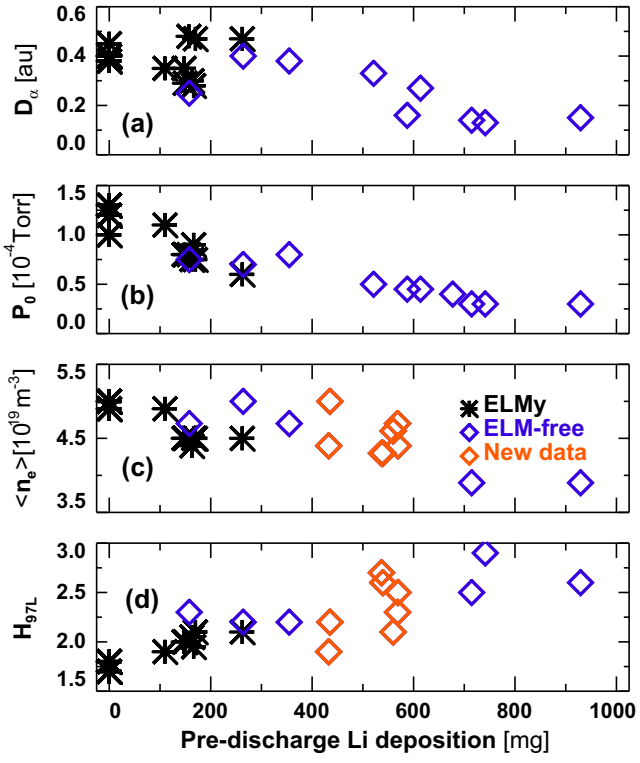

Fig. 1. Global plasma parameters suggest recycling decreased and performance increased nearly continuously with increasing lithium deposition. As a function of pre-discharge lithium deposition, (a) lower divertor D_α emission at ~0.3 s, (b) midplane fast ion gauge neutral pressure P_0 at ~0.3 s, (c) line-averaged density from Thomson scattering $\langle n_e \rangle$ at 0.4 s, and (d) EFIT02 confinement time normalized by ITER97L scaling, at time of peak W_{MHD}. Data is from ELMy discharges (black *), partly or fully ELM-free discharges in original gradual lithium scan (blue ◇), and fully ELM-free discharges in more recent experiments (orange ◇). (For interpretation of the references to color in this figure legend, the reader is referred to the web version of this article.)

The improvement in global confinement with increasing lithium deposition was closely related to a higher pressure pedestal, which itself reflected a number of changes in the pedestal structure. The pedestal structure is quantified using the fitting parameters of the modified hyperbolic tangent (mtanh) function, while profile values at fixed values of normalized poloidal flux (ψ_N) come from spline fits. Details of the pedestal analysis methods can be found in previous work [17]. ELM suppression with lithium coatings was shown to coincide with a shift of the density pedestal away from the separatrix, as well as significant increase in its width. By shifting the peak density gradient away from the separatrix, lithium reduced the bootstrap current at the edge (where it had the largest effect on stability), suppressing ELMs [14,17]. With inclusion of the additional data in Fig. 2a and b, it is now apparent that the density pedestal shifted and widened continuously with increasing lithium deposition, even after ELMs were completely suppressed. Just as in the earlier work, there was no significant trend in the temperature pedestal width or symmetry point (not shown), so the pressure pedestal (also not shown) mostly followed the same trend as the density.

Fig. 2c–h shows the profile values near the pedestal top ($\psi_N = 0.8$). Values at fixed ψ_N from spline fits are used due to the difficulty of fitting ultra-wide ELM-free pressure pedestals with the mtanh function. Though electron density n_e at the pedestal top (not shown) did not systematically change, electron temperature T_e and pressure p_e increased nearly continuously, even after ELMs were suppressed. While the changes in pedestal structure and increases in total pressure and stored energy were dominated by the electrons, the ion profiles also showed continuous dependence on lithium deposition – again, even after ELMs were completely suppressed. Fig. 2e–g shows that ion density n_i decreased with increasing lithium, while toroidal rotation v_{tor} and ion temperature T_i increased. Much of the scatter in the data – rotation especially – was due to variations in beam power. These data are from the pedestal top, but the same trends continued near the edge ($\psi_N = 0.95$). The trends in n_i and T_i partly canceled, causing ion pressure p_i to increase with lithium at the pedestal top in Fig. 2h and decrease with lithium near the edge (not shown). As the changes to the p_i profile were similar to the changes in p_e, only smaller in magnitude, trends in the total pressure pedestal mirrored those in p_e.

3. Evolution with time

A key part of understanding how lithium affects the plasma is to determine how its effects change with time. As the discharge continues and the impinging deuterons bond with lithium, less unbound lithium remains. In principle, the lithium could saturate as the total fluence increases, in which case recycling would increase with time. This effect was not seen in this experiment. Fig. 3 compares D_α measurements in a pre-Li ELMy discharge (black) and a with-Li ELM-free discharge. These measurements were made using an absolutely calibrated filtered 1-D CCD camera [21]. While D_α

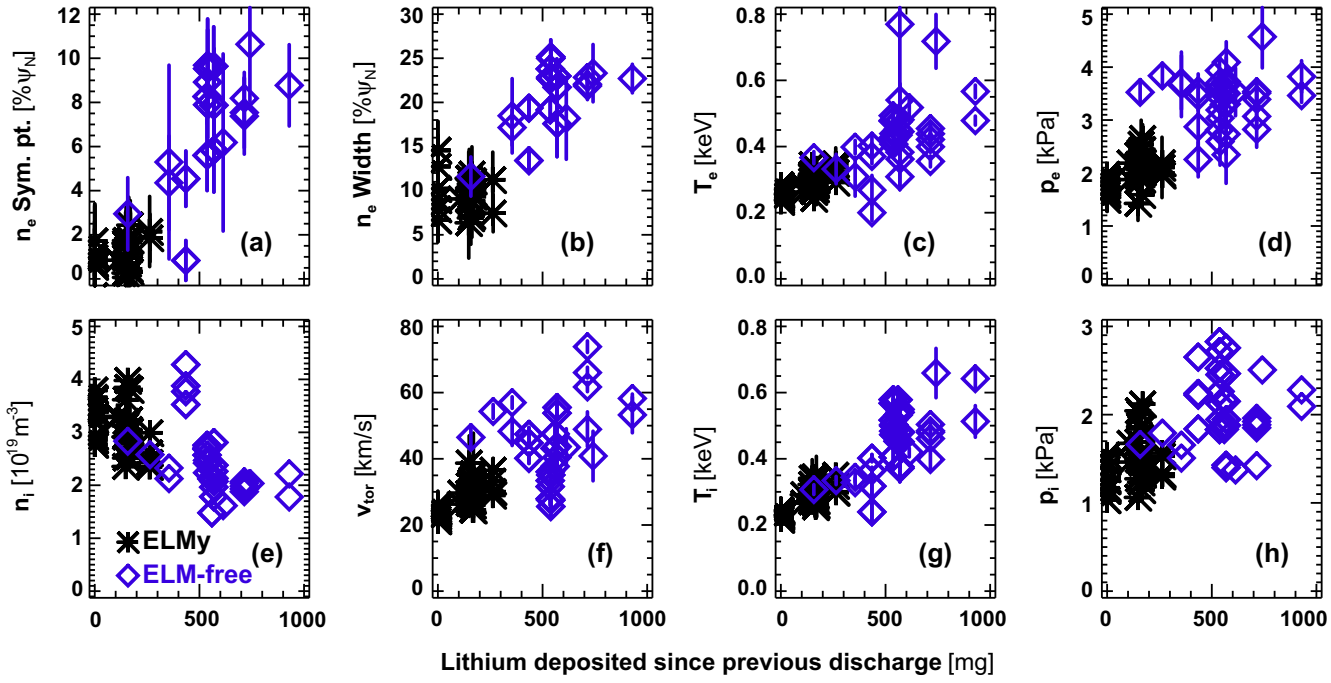

Fig. 2. Pedestal profiles evolved with increasing lithium, even after ELM suppression. As a function of pre-discharge lithium deposition, (a) symmetry point and (b) full width of modified hyperbolic tangent (mtanh) fits to pedestal profiles of electron density n_e; profile values at $\psi_N = 0.8$ from spline fits of, (c) electron temperature T_e, (d) electron pressure p_e, (e) ion density n_i, (f) toroidal rotation velocity v_{tor}, (g) ion temperature T_i, and (h) ion pressure p_i. Profiles were measured during ELMy phases (black *) and ELM-free phases (blue ◇). (For interpretation of the references to color in this figure legend, the reader is referred to the web version of this article.)

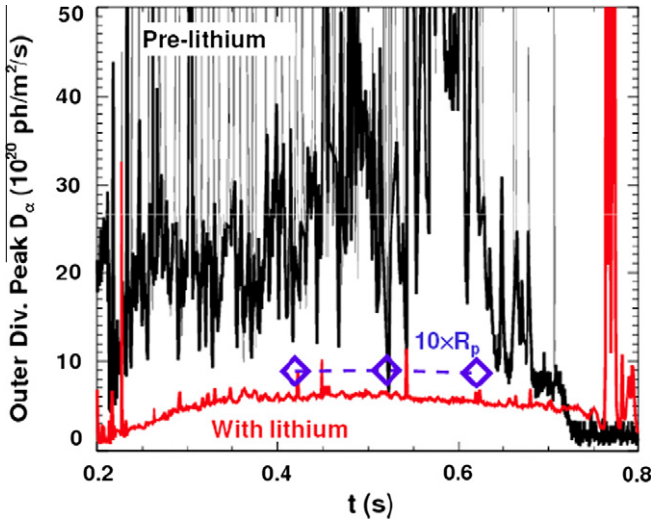

Fig. 3. D_α emission was approximately constant with time in ELM-free discharge. Time traces of outer divertor peak D_α emission for a pre-lithium ELMy discharge (black), a with-lithium ELM-free discharge (red), and inferred recycling coefficient R_p from the ELM-free discharge, magnified by 10 (blue ◇). (For interpretation of the references to color in this figure legend, the reader is referred to the web version of this article.)

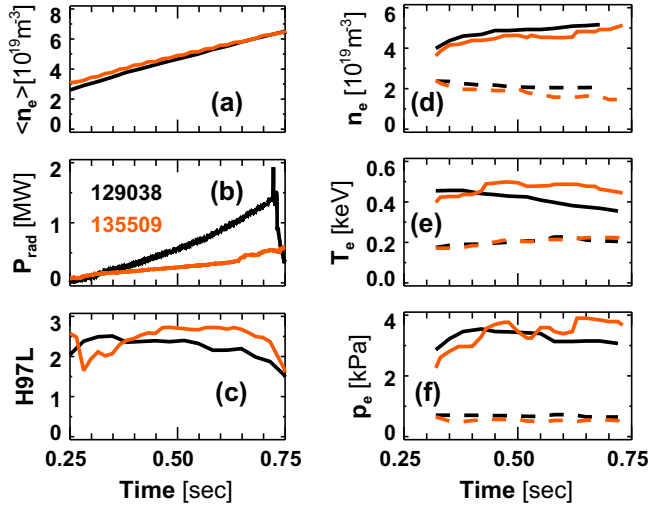

Fig. 4. Temporal variation of ELM-free pedestal was modest relative to evolution of global parameters. For two ELM-free discharges, one from the original experiment (black) and one from the newer one (orange), time traces of (a) line-averaged density from Thomson scattering $\langle n_e \rangle$, (b) total radiated power P_{rad}, (c) confinement time normalized by ITER97L scaling, and profile values at $\psi_N = 0.8$ (solid) and $\psi_N = 0.95$ (dashed) from spline fits of (d) electron density n_e, (e) electron temperature T_e, and (f) electron pressure p_e. (For interpretation of the references to color in this figure legend, the reader is referred to the web version of this article.)

emission increased with time in the ELMy discharges, it was nearly constant or decreased slightly in the ELM-free discharges.

In addition to recycling, D_α emission is dependent on scrape-off layer (SOL) density and temperature, which could have evolved with time as average density and radiated power increased, as seen in Fig. 4a and b. However, Fig. 4c–e shows that the variation of the pedestal parameters with time was relatively small, both near the top ($\psi_N = 0.8$, solid) and near the edge ($\psi_N = 0.95$, dashed). Despite a near doubling of line-averaged density and large increases in radiated power, at the pedestal top density increased and temperature decreased only ~20%. At the edge, density actually decreased and temperature increased, neither of which are consistent with an increase in recycling.

To quantitatively determine the time evolution of the divertor recycling coefficient, SOLPS interpretive modeling [22] was employed; details of the modeling technique are given elsewhere

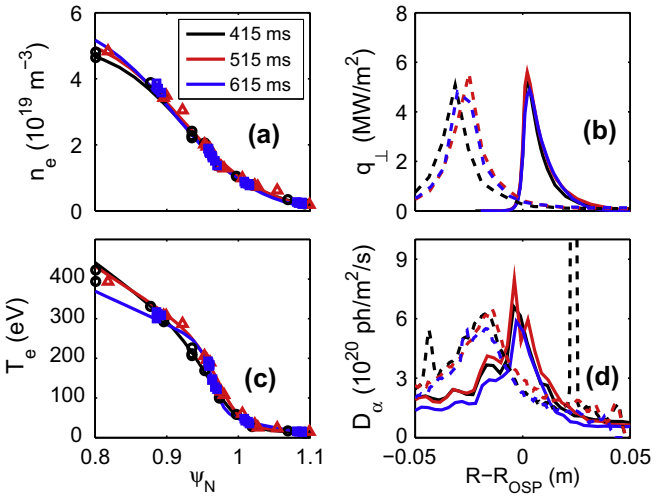

Fig. 5. Measured and calculated SOL profiles and inferred recycling coefficients showed little variation with time. Profiles shown for (a) electron density n_e, (b) electron temperature T_e, (c) lower divertor heat flux $q^\perp$, and (d) lower divertor D_α emission. Measurements are shown as symbols and dashed lines; SOLPS calculations shown as solid lines. Measurements were made in 70 ms windows centered at 415 ms (black ○), 515 ms (red △), and 615 ms (blue □). The measured and calculated $q^\perp$ and D_α peaks do not align perfectly due to error in the equilibrium reconstruction at the outer strike point. (For interpretation of the references to color in this figure legend, the reader is referred to the web version of this article.)

[15,16]. Briefly, the particle and energy diffusivities were varied iteratively to match the n_e and T_e profiles while the separatrix location and recycling coefficient were constrained by the peak values (not the profiles) of heat flux $q^\perp$ and D_α emission. Fig. 5 shows measured (symbols and dashed lines) and calculated (solid lines) profiles of SOL (a) density n_e, (b) temperature T_e, (c) $q^\perp$, and (d) D_α emission for three different times in an ELM-free discharge. Just from the raw data, it is clear that the SOL profiles varied only modestly despite line-averaged density increasing by ~40% between the black and blue curves. Indeed, the inferred recycling coefficients at 415, 515, and 615 ms were approximately constant at 0.89, 0.90, and 0.87, respectively.

4. Discussion

Previous work [18,19] demonstrated that recycling declined continuously with additional lithium, though the cause remains unclear, as even the thinnest coatings were several times the ion implantation depth. It is well established that lithium reduces recycling by bonding deuterons, but it is unknown precisely how this process depends on lithium thickness and uniformity, or the precise roles of erosion, redeposition, passivation by deuterium and residual gases, or chemistry with carbon, oxygen, and/or other elements. Some of these issues and efforts underway to understand them were discussed in [19].

Given the continuous reduction in recycling with increasing lithium coatings, a simple explanation for the continuous reduction in transport as ELMs were suppressed [16,18,19] could be a gradual shift in the peeling–ballooning boundary that limited growth of the transport barrier. However, this does not explain the improved confinement and evolution of the pedestal with additional lithium even after ELMs were suppressed and the pedestal was no longer limited by peeling–ballooning modes. Efforts are underway to determine what set the maximum pedestal width and height in the ELM-free regime, why it continued to grow with additional lithium after ELMs were suppressed, and to more completely explain the concurrent changes in recycling, ELM stability, transport, and pedestal structure due to lithium coatings in NSTX.

While the ELM-free H-mode pedestal profiles evolved with additional lithium, their temporal variations were small relative to the global increases in average density and radiative losses from impurities. The relatively steady pedestal profiles are even more intriguing when considering the natural growth of the pedestal in other ELM-free regimes, or the possible saturation of the lithium coatings. In fact, we have shown that the low-recycling properties of lithium were not significantly degraded on the timescale of these discharges, as neither D_α emission nor the recycling coefficient increased with time. The possibility of controlling the ELM-free H-mode pedestal profile in a relatively steady state has positive implications for longer pulse machines that will use lithium coatings, including the NSTX-Upgrade [23].

Acknowledgements

This research was supported in part by the US Department of Energy under contracts DE-AC05-00OR22725, DE-AC02-09CH11466 and DE-FC02-04ER54698. We gratefully acknowledge the contribution of the NSTX technical and operations staff, and measurements made by V.A. Soukhanovskii, R. Raman, B.P. LeBlanc, S.A. Sabbagh, R.E. Bell, and S. Paul.

References

[1] S.I. Krasheninnikov, L.E. Zakharov, G.V. Pereverzev, Phys. Plasmas 10 (2003) 1678.
[2] M. Ono, S.M. Kaye, Y.-K.M. Peng, et al., Nucl. Fusion 40 (2000) 557–561.
[3] D.K. Mansfield, K.W. Hill, J.D. Strachan, et al., Phys. Plasmas 3 (1996) 1892.
[4] R. Majeski, R. Doerner, T. Gray, et al., Phys. Rev. Lett. 97 (2006) 075002.
[5] H.W. Kugel, M.G. Bell, R. Bell, et al., J. Nucl. Mater. 363–365 (2007) 791–796.
[6] H.W. Kugel, M.G. Bell, J.-W. Ahn, et al., Phys. Plasmas 15 (2008) 056118.
[7] H.W. Kugel, M.G. Bell, H. Schneider, et al., Fusion Eng. Des. 85 (2010) 865–873.
[8] H.W. Kugel, D. Mansfield, R. Maingi, et al., J. Nucl. Mater. 390–391 (2009) 1000–1004.
[9] D.K. Mansfield, H.W. Kugel, R. Maingi, et al., J. Nucl. Mater. 390–391 (2009) 764–767.
[10] M.G. Bell, H.W. Kugel, R. Kaita, et al., Plasma Phys. Control. Fusion 51 (2009) 124054.
[11] J.M. Canik, R. Maingi, T.E. Evans, et al., Phys. Rev. Lett. 104 (2010) 045001.
[12] J.M. Canik, A.C. Sontag, R. Maingi, et al., Nucl. Fusion 50 (2010) 064016.
[13] V.A. Soukhanovskii, J.-W. Ahn, R.E. Bell, et al., Nucl. Fusion 51 (2011) 012001.
[14] R. Maingi, T.H. Osborne, B.P. LeBlanc, et al., Phys. Rev. Lett. 103 (2009) 075001.
[15] J.M. Canik, R. Maingi, S. Kubota, et al., Phys. Plasmas 18 (2011) 056118.
[16] J.M. Canik, R. Maingi, V.A. Soukhanovskii, et al., J. Nucl. Mater. 415 (2011) S409–S412.
[17] D.P. Boyle, R. Maingi, P.B. Snyder, et al., Plasma Phys. Control. Fusion 53 (2011) 105011.
[18] R. Maingi, S.M. Kaye, C.H. Skinner, et al., Phys. Rev. Lett. 107 (2011) 145004.
[19] R. Maingi, D.P. Boyle, J.M. Canik, et al., Nucl. Fusion 52 (2012) 083001.
[20] S.M. Kaye, M. Greenwald, U. Stroth, et al., Nucl. Fusion 37 (1997) 1303–1328.
[21] V.A. Soukhanovskii, A.L. Roquemore, C.H. Skinner, et al., Rev. Sci. Instrum. 74 (2003) 2094.
[22] R. Schneider, X. Bonnin, K. Borrass, et al., Contrib. Plasma Phys. 46 (2006) 3–191.
[23] J.E. Menard, S. Gerhardt, M. Bell, et al., Nucl. Fusion 52 (2012) 083015.